Theory and Numerical Calculations for Radially Inhomogeneous Circular Ferrite Circulators

Clifford M. Krowne, *Senior Member, IEEE*, and Robert E. Neidert, *Member, IEEE*

Abstract—**This paper presents a new theory for the operation of microstrip and stripline circulators, specially set up to permit radial variation of all the magnetic parameters. A computer code, taking only a few seconds per calculated point on a modest computer, was developed from the theory, and calculated results are given. In the theory we develop a two-dimensional (2-D) recursive Green's function G suitable for determining the electric field E_z anywhere within a microstrip or stripline circulator. The recursive nature of G is a reflection of the inhomogeneous region being broken up into one inner disk containing a singularity and N annuli. G has the correct properties to allow matching to the external ports, thereby enabling s-parameters to be found for a three-port ferrite circulator. Because of the general nature of the problem construction, the ports may be located at arbitrary azimuthal angle ϕ and possess arbitrary line widths. Inhomogeneities may occur in the applied magnetic field $H_{\rm app}$, magnetization $4\pi M_s$, and demagnetization factor N_d. All magnetic inhomogeneity effects can be put into the frequency dependent tensor elements of the anisotropic permeability tensor. Numerical results are presented for the simpler but immensely practical case of symmetrically disposed ports of equal widths taking into account these radial inhomogeneities. Studies of breaking up the area into 1, 2, and 5 annuli are undertaken to treat specific inhomogeneous problems. The computer code which evaluates the recursive Green's function is very efficient and has no convergence problems.**

I. Introduction

THE ferrite community has long needed a simple but accurate way to calculate circulator performance in the presence of radial variation of bias field, ferrite material type, and demagnetizing factor. Full analysis with finite element or finite difference methods is so slow, user-unfriendly, and expensive that generally useful answers about the affects of radial variations have not been forthcoming. The paper here provides a means to get these answers, at the rate of a few seconds per calculation point, with a computer code developed from a new partial mode matching theory.

Previous work in the area of multiport circulators has focused on the treatment of high-symmetry geometric configurations, a limited number of symmetrically disposed ports, and a homogeneous nonreciprocating medium [1]–[15]. The theoretical techniques for modeling the circulator have ranged from Green's functions, boundary element methods, boundary contour integral methods, to finite element methods. Each method has special advantages and disadvantages in relation to the other methods, depending upon what the researcher is interested in emphasizing in the problem. Discussion of these numerical techniques as well as other information on circulators and anisotropic media may be found in recent surveys [16], [17].

Our interest is in obtaining a formulation which allows us to inspect the physics and electromagnetics of the solution, and which can be related to earlier simple results on homogeneous problems. We also want a solution which is numerically efficient to evaluate. With these considerations, an analytical approach was taken to derive a Green's function which would allow the circulator region to be divided up into an arbitrary number of rings of definite radial thickness. The idea was to make the rings or annuli thin enough to accurately describe the actual arbitrary radial variation of the various inhomogeneities contributing to the permeability tensor.

In Sections II and III we develop a two-dimensional (2-D) recursive Green's function G suitable for determining the electric field E_z anywhere within the circulator. The recursive nature of G is a reflection of the inhomogeneous region being broken up into one inner disk, containing a singularity, and N annuli. G has the correct properties to allow matching to the external ports, thereby enabling s-parameters to be found for a three-port ferrite circulator. Because of the general nature of the problem construction, the ports may be located at arbitrary azimuthal angle ϕ_i and possess arbitrary line widths w_i for the ith port. The line widths may be also measured in terms of the angular spread $\Delta\phi_i$ on the outer edge of the circular disk of radius R. Inhomogeneities occur in the applied magnetic field $H_{\rm app}$, magnetization $4\pi M_s$, and demagnetization factor N_d. All magnetic inhomogeneity effects can be put into the frequency dependent tensor elements of the anisotropic permeability tensor. The process of how this can be done will be discussed in Section V.

Section VI gives some calculated results for a few arbitrarily selected cases of radially nonuniform demagnetizing factor, applied bias field, and ferrite material types. These calculations are for the immensely practical case of symmetrically disposed ports of equal widths. Studies of breaking up the area into 1, 2, and 5 annuli are undertaken to display the approximation levels required to treat inhomogeneous problems. The computer code, which evaluates the recursive Green's function, is very efficient and calculation time is presented.

II. Theory

The Green's function to be developed below, although of a recursive nature, may in the limit be shown to reduce to

Manuscript received April 9, 1995; revised November 27, 1995.

The authors are with the Microwave Technology Branch, Electronics Science & Technology Division, Naval Research Laboratory, Washington, DC 20375-5347 USA.

Publisher Item Identifier S 0018-9480(96)01545-1.

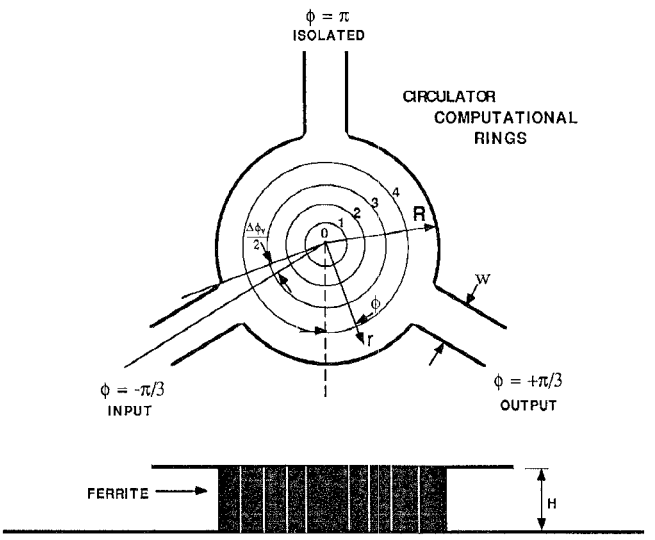

Fig. 1. Top view of a radially inhomogeneous circulator showing the inner disk labeled with index number $\imath = 0$ and the annuli indexed from $\imath = 1$ onward. Here four annuli are shown. The figure shows the special case of symmetrically disposed ports located at $\phi = -\pi/3$ (input), $\pi/3$ (output), and π (isolated). Angular port width is $\Delta\phi_\imath$. A side view is shown also for a real physical circulator. Biased ferrite material of thickness H exists only for $\imath \leq R$.

either the single circular disk case [18], [19] or a circular ring [20]–[22]. We develop the Green's function as a response to a forcing function which represents a driving function, or source function, of magnetic field type, $H_{\phi s}$, located on the azimuthal boundary of a circular contour of radius R. Fig. 1 shows the general geometric configuration of the circulator. The forcing function has the property of limiting the field to finite values only at radius $r = R$ and azimuthal angle locations $\phi = \phi_i$, where i represents specific points along the enclosing circulator contour. The linear system of partial differential equations (PDE's), through which $H_{\phi s}(r = R, \phi = \phi_i)$ imposes its forcing behavior, may be written formally in terms of one governing PDE with operator L acting on our prime field quantity of interest here, E_z

$$LE_z(r, \phi) = H_{\phi s}(R, \phi_i). \tag{1}$$

From E_z, the other field components, H_ϕ and H_r, can be determined in this 2-D problem.

Let us identify the magnetic field at location $r = R$ to be the contour field associated with the surface in the 2-D problem we are treating

$$H_{\phi c}(R, \phi) = H_\phi(R, \phi) \tag{2}$$

where an explicit subscript is added to denote this association. $H_{\phi c}$ may be related to the physical forcing magnetic field $H_{\phi s}$ by the relation

$$\delta(r - R)H_{\phi c}(R, \phi) = H_{\phi s}(R, \phi). \tag{3}$$

Using the properties of the Dirac delta function in the spatial radial direction and the azimuthal angular direction, we find

$$E_z(r, \phi) = \int_{-\pi}^{\pi} G_{\mathrm{EH}}(r, \phi; R, \phi')H_{\phi c}(R, \phi')d\phi'. \tag{4}$$

It is the Green's function $G_{\mathrm{EH}}(r, \phi; R, \phi')$ at $r = R$ which we are particularly interested in obtaining in this paper so that the s-parameters may be found for the three-port inhomogeneous circulator. The recursion process to be employed here is like that utilized for planar structures [23].

Maxwell's sourceless curl equations are, for harmonic conditions with phasor time dependence $\exp(\imath\omega t)$ assumed

$$\nabla \times \mathbf{E} = -\imath\omega\mathbf{B} \tag{5}$$

$$\nabla \times \mathbf{H} = \imath\omega\mathbf{D}. \tag{6}$$

These two equations are valid within the ferrite disk region which is considered to be inhomogeneously loaded with material (the disk could also be a magnetically biased semiconductor region displaying the magnetoplasma effect). The constitutive relationships are given generally by

$$\mathbf{B} = \hat{\mu}\mathbf{H} \tag{7}$$

$$\mathbf{D} = \hat{\varepsilon}\mathbf{E}. \tag{8}$$

In the ferrite disk region, we will assume that the dielectric tensor reduces to a scalar

$$\hat{\varepsilon} = \varepsilon. \tag{9}$$

Of course, this would not be the case for a semiconductor where we would retain the tensor permittivity and drop the tensor permeability [24], [25].

The general expression in matrix notation for the curl of an arbitrary vector field in cylindrical coordinates is

$$\nabla \times \mathbf{A} = \frac{1}{r}\begin{vmatrix} \hat{r} & r\hat{\phi} & \hat{z} \\ \partial_r & \partial_\phi & \partial_z \\ A_r & rA_\phi & A_z \end{vmatrix} \tag{10}$$

where it is noted that the expansion of (10) is accomplished by keeping the unit vector terms outside of the partial operators ∂_i, $i = r, \phi, z$. It is also noted that we use r instead of the usual ρ for the cylindrical radius. For the 2-D problem we are constructing, it is sufficient to drop a dimension by setting

$$\frac{\partial}{\partial z} = 0. \tag{11}$$

To be somewhat consistent with notation in the circulator literature [18], we set the permeability tensor

$$\hat{\mu} = \begin{bmatrix} \mu & -\imath\kappa & 0 \\ \imath\kappa & \mu & 0 \\ 0 & 0 & \mu_0 \end{bmatrix}. \tag{12}$$

By (7) and (12)

$$\mathbf{B} = \hat{\mu}\mathbf{H} = \begin{bmatrix} \mu & -\imath\kappa & 0 \\ \imath\kappa & \mu & 0 \\ 0 & 0 & \mu_0 \end{bmatrix}\begin{bmatrix} H_r \\ H_\phi \\ H_z \end{bmatrix} = \begin{pmatrix} \mu H_r - \imath\kappa H_\phi \\ \imath\kappa H_r + \mu H_\phi \\ \mu_0 H_z \end{pmatrix}. \tag{13}$$

Solving for H_ϕ and H_r in terms of partial derivatives of E_z

$$H_\phi = \frac{1}{\imath\omega(\mu^2 - \kappa^2)}\left[\frac{\imath\kappa}{r}\frac{\partial E_z}{\partial\phi} + \mu\frac{\partial E_z}{\partial r}\right] \tag{14}$$

$$H_r = \frac{1}{\omega(\mu^2 - \kappa^2)}\left[\frac{\imath\mu}{r}\frac{\partial E_z}{\partial\phi} + \kappa\frac{\partial E_z}{\partial r}\right]. \tag{15}$$

The governing Helmholtz equation for this problem is

$$\nabla^2 E_z + k_{\text{eff}}^2 E_z = 0 \tag{16}$$

with the definitions

$$k_{\text{eff}}^2 = \omega^2 \varepsilon \mu_{\text{eff}} \tag{17}$$

$$\mu_{\text{eff}} = \frac{\mu^2 - \kappa^2}{\mu}. \tag{18}$$

Using definition (18) in (14) and (15) provides substantially more compact expressions for H_ϕ and H_r

$$H_\phi = \frac{1}{i\mu_{\text{eff}}}\left[\frac{i\kappa}{\mu}\frac{1}{r}\frac{\partial E_z}{\partial \phi} + \frac{\partial E_z}{\partial r}\right] \tag{19}$$

$$H_r = \frac{1}{\omega\mu_{\text{eff}}}\left[\frac{i}{r}\frac{\partial E_z}{\partial \phi} + \frac{\kappa}{\mu}\frac{\partial E_z}{\partial r}\right]. \tag{20}$$

A. E_z and H_ϕ Fields in the Inner Disk

The inhomogeneous circular surface is broken up into one inner disk centered at $r = 0$, and N annuli, each annulus labeled by index i. To be consistent in labeling notation, the inner disk is labeled with $i = 0$. The disk, and each annulus region is sourceless, so that the homogeneous Helmholtz equation (16) holds. The solution to (16) in cylindrical coordinates is well known to be Bessel functions multiplied by azimuthal circular harmonics. For the problem at hand, azimuthal symmetry exists, requiring that the separable circular harmonics be of type $\{\exp(in\phi)\}$, for any integer n. Helmholtz equation (16) will therefore yield Bessel functions of integer order. Because the inner disk contains the point $r = 0$, the only Bessel function to be well behaved, not possessing a singularity, will be the Bessel function of the first kind, J_n. Therefore the total electric field E_{z0} in the disk must be a superposition of

$$E_{zn0} = a_{n0} J_n(k_{\text{eff},0} r) e^{in\phi} \tag{21}$$

giving

$$E_{z0} = \sum_{n=-\infty}^{\infty} E_{zn0} = \sum_{n=-\infty}^{\infty} a_{n0} J_n(k_{\text{eff},0} r) e^{in\phi}. \tag{22}$$

Likewise for the magnetic fields, invoking (19)

$$H_{\phi 0} = \sum_{n=-\infty}^{\infty} -\frac{i}{\omega\mu_{\text{eff},0}} a_{n0} \times \left[k_{\text{eff},0} J_n'(k_{\text{eff},0} r) - \frac{n\kappa_0}{\mu_0}\frac{1}{r} J_n(k_{\text{eff},0} r)\right] e^{in\phi}. \tag{23}$$

To standardize the notation, abbreviate, and make transparent what is happening in the recursion process itself, a few definitions are made (the upper index on C is the component, and the lower indices are azimuthal mode number, field type, Bessel function type, and ring index)

$$C_{neai}(r) \equiv J_n(k_{\text{eff},i} r) \tag{24}$$

$$c_i \equiv -\frac{i}{\omega\mu_{\text{eff},i}} \tag{25}$$

$$C^{\phi}_{nhai}(r) = c_i\left[k_{\text{eff},i} J_n'(k_{\text{eff},i} r) - \frac{n\kappa_i}{\mu_i}\frac{1}{r} J_n(k_{\text{eff},i} r)\right]. \tag{26}$$

In these three definition equations, the general disk or annulus location index i has been used as the last index on the C_{neai} and C_{nhai}, on the material tensor element parameters μ_i and κ_i, and on the effective propagation constant $k_{\text{eff},i}$ and permeability $\mu_{\text{eff},i}$. For the inner disk, the index in (24)–(26) is merely $i = 0$, allowing us to rewrite (22) and (23) as

$$E_{z0} = \sum_{n=-\infty}^{\infty} a_{n0} C_{nea0}(r) e^{in\phi} \tag{27}$$

$$H_{\phi 0} = \sum_{n=-\infty}^{\infty} a_{n0} C^{\phi}_{nha0}(r) e^{in\phi}. \tag{28}$$

B. Fields in the Annuli

Because an annulus does not include the origin, a superposition of any two linearly independent Bessel functions will be required to construct the radial part of the separable solution to (16). The electric field is therefore

$$E_{zi} = \sum_{n=-\infty}^{\infty} [a_{ni} J_n(k_{\text{eff},i} r) + b_{ni} N_n(k_{\text{eff},i} r)] e^{in\phi}; \quad i = 1, 2, \ldots, N. \tag{29}$$

As in (24), let us define

$$C_{nebi}(r) \equiv N_n(k_{\text{eff},i} r) \tag{30}$$

so that (29) can be rewritten in the more abbreviated and transparent form

$$E_{zi} = \sum_{n=-\infty}^{\infty} [a_{ni} C_{neai}(r) + b_{ni} C_{nebi}(r)] e^{in\phi}; \quad i = 1, 2, \ldots, N. \tag{31}$$

For the $H_{\phi i}$ field component, referring to (19)

$$H_{\phi i} = \sum_{n=-\infty}^{\infty} c_i a_{ni}\left[k_{\text{eff},i} J_n'(k_{\text{eff},i} r) - \frac{n\kappa_i}{\mu_i}\frac{1}{r} J_n(k_{\text{eff},i} r)\right] e^{in\phi} + \sum_{n=-\infty}^{\infty} c_i b_{ni}\left[k_{\text{eff},i} N_n'(k_{\text{eff},i} r) - \frac{n\kappa_i}{\mu_i}\frac{1}{r} N_n(k_{\text{eff},i} r)\right] e^{in\phi}. \tag{32}$$

Using the coefficient definition in (26) for the a_{ni} factor and the additional definition

$$C^{\phi}_{nhbi}(r) = c_i\left[k_{\text{eff},i} N_n'(k_{\text{eff},i} r) - \frac{n\kappa_i}{\mu_i}\frac{1}{r} N_n(k_{\text{eff},i} r)\right]. \tag{33}$$

$H_{\phi i}$ can be expressed in the much more compact form

$$H_{\phi i} = \sum_{n=-\infty}^{\infty} \left[a_{ni} C^{\phi}_{nhai}(r) + b_{ni} C^{\phi}_{nhbi}(r)\right] e^{in\phi}. \tag{34}$$

C. Boundary Conditions and the Disk—First Annulus Interface

There are three distinct types of boundary condition interfaces. The first boundary condition type is at the disk—first annulus interface. This interface must match the inner disk, which contains a potential singularity at $r = 0$ which has been specially excluded, to the first annulus which contains two linearly independent Bessel functions out of which the E_z field is constructed.

Once the matching has been completed at this first interface, the field information can be pulled through to the next interface, and the matching procedure repeated. Thus, each internal interface due to two adjacent annuli involves the same matching process. These internal interfaces constitute the second type of boundary condition. If there are N annuli, then there will be exactly $N_i = N-1$ interfaces of the second type.

The third type of boundary condition occurs at the interface between the last annulus, the $i = N$ annulus, and the external part of the circulator geometry. This is where the last annulus or ring abuts or touches either an ideally imposed magnetic wall, which approximately expresses the transition between the ferrite material and the outside dielectric (air or a surrounding dielectric), or the transition ports taking energy into or out of the circulator. For a three-port circulator, these ports are referred to as the input port, the output port, and the isolated port. Normal practical design strategy attempts to minimize the exiting signal from the isolated port and maximize the exiting signal from the output port.

There will be a total of $N_i + 2$ interfacial boundary conditions, all of the internal ones plus one disk-annulus interface and one Nth annulus-outside interface. The inner disk has radius r_0. Each annulus has radius r_i measured from its center. The width of each annulus is $\Delta r_i = r_{iO} - r_{iI}$, where the subscript "$O$" or "$I$" indicates outer or inner radius of the ith annulus.

It is sufficient to apply boundary constraints on either the (B_n, D_n) normal pair or the (E_t, H_t) tangential pair. We choose the second pair as it is easily applied. For the first type of interfacial boundary condition

$$E_{z0}(r = r_0) = E_{z1}(r = r_{1I}) \tag{35}$$

$$H_{\phi 0}(r = r_0) = H_{\phi 1}(r = r_{1I}). \tag{36}$$

Using (27) and (31) for the E_z constraint, (35) becomes

$$\sum_{n=-\infty}^{\infty} a_{n0} C_{nea0}(r_0) e^{in\phi} = \sum_{n=-\infty}^{\infty} [a_{n1} C_{nea1}(r_{1I}) + b_{n1} C_{neb1}(r_{1I})] e^{in\phi}. \tag{37}$$

Utilizing (28) and (34) for the H_ϕ constraint, (36) becomes

$$\sum_{n=-\infty}^{\infty} a_{n0} C^{\phi}_{nha0}(r_0) e^{in\phi} = \sum_{n=-\infty}^{\infty} \left[a_{n1} C^{\phi}_{nha1}(r_{1I}) + b_{n1} C^{\phi}_{nhb1}(r_{1I})\right] e^{in\phi}. \tag{38}$$

By the orthogonality of the azimuthal harmonics on $(-\pi, \pi)$, these equations may be written down for each individual nth harmonic

$$a_{n0} C_{nea0D} = a_{n1} C_{nea1D} + b_{n1} C_{neb1D} \tag{39a}$$

$$a_{n0} C^{\phi}_{nha0D} = a_{n1} C^{\phi}_{nha1D} + b_{n1} C^{\phi}_{nhb1D}. \tag{39b}$$

Here the argument information of the C coefficients has been compressed into a single added subscript index D which denotes radial evaluation at the disk radius $D = r_0 = r_{1I}$. Solution of (39) yields for the 1st annulus field coefficients a_{n1} and b_{n1}

$$a_{n1} = \frac{\begin{vmatrix} C_{nea0D} & C_{neb1D} \\ C_{nha0D} & C_{nhb1D} \end{vmatrix}}{\begin{vmatrix} C_{nea1D} & C_{neb1D} \\ C_{nha1D} & C_{nhb1D} \end{vmatrix}} a_{n0} \tag{40a}$$

$$b_{n1} = \frac{\begin{vmatrix} C_{nea1D} & C_{nea0D} \\ C_{nha1D} & C_{nha0D} \end{vmatrix}}{\begin{vmatrix} C_{nea1D} & C_{neb1D} \\ C_{nha1D} & C_{nhb1D} \end{vmatrix}} a_{n0}. \tag{40b}$$

These expressions may be considerably abbreviated by defining the disk-to-annulus coupling numerator factors

$$M_{DAa} = \begin{vmatrix} C_{nea0D} & C_{neb1D} \\ C_{nha0D} & C_{nhb1D} \end{vmatrix}, \tag{41a}$$

$$M_{DAb} = \begin{vmatrix} C_{nea1D} & C_{nea0D} \\ C_{nha1D} & C_{nha0D} \end{vmatrix} \tag{41b}$$

and the determinant D_i providing the information in the ith annulus

$$D_i = \begin{vmatrix} C_{neaiA} & C_{nebiA} \\ C_{nhaiA} & C_{nhbiA} \end{vmatrix}. \tag{42}$$

In (42), subscript combination iA denotes a radial evaluation at the ith annulus inner radius r_{iI}, that is

$$r_{iA} = r_{iI} = r_i - \Delta r_i/2. \tag{43}$$

Thus, we may now write a_{n1} and b_{n1} as

$$a_{n1} = \frac{M_{DAa}}{D_1} a_{n0} \tag{44a}$$

$$b_{n1} = \frac{M_{DAb}}{D_1} a_{n0}. \tag{44b}$$

D. Intra-Annuli Boundary Conditions

The (E_t, H_t) tangential pair is used to match between two adjacent annuli. Following forms (35) and (36)

$$E_{zi}(r = r_{iO}) = E_{z(i+1)}(r = r_{(i+1)I}) \tag{45}$$

$$H_{\phi i}(r = r_{iO}) = H_{\phi(i+1)}(r = r_{(i+1)I}). \tag{46}$$

Invoking the annuli E_z field expression in (31), and inserting it into (45)

$$a_{ni} C_{neai}(r_{iO}) + b_{ni} C_{nebi}(r_{iO}) = a_{n(i+1)} C_{nea(i+1)}(r_{(i+1)I}) + b_{n(i+1)} C_{neb(i+1)}(r_{(i+1)I}). \tag{47}$$

Similarly, for H_ϕ recalling (34), and inserting into (46)

$$a_{ni} C^{\phi}_{nhai}(r_{iO}) + b_{ni} C^{\phi}_{nhbi}(r_{iO}) = a_{n(i+1)} C^{\phi}_{nha(i+1)}(r_{(i+1)I}) + b_{n(i+1)} C^{\phi}_{nhb(i+1)}(r_{(i+1)I}). \tag{48}$$

These two equations may be compressed by defining the fifth index on the C coefficients to be the outer radius r_{iO} of the ith annulus or the inner radius $r_{(i+1)I}$ of the $(i+1)$th annulus. This so defined radius is precisely the value used to evaluate the radial arguments of the C coefficients

$$a_{ni}C_{neaii} + b_{ni}C_{nebii} = a_{n(i+1)}C_{nea(i+1)i} + b_{n(i+1)}C_{neb(i+1)i} \quad (49a)$$

$$a_{ni}C^{\phi}_{nhaii} + b_{ni}C^{\phi}_{nhbii} = a_{n(i+1)}C^{\phi}_{nha(i+1)i} + b_{n(i+1)}C^{\phi}_{nhb(i+1)i}. \quad (49b)$$

This set of equations can be solved for the $(i+1)$th annulus field coefficients $a_{n(i+1)}$ and $b_{n(i+1)}$

$$a_{n(i+1)} = \frac{\begin{vmatrix} L_{neii} & C_{neb(i+1)i} \\ L_{nhii} & C_{nhb(i+1)i} \end{vmatrix}}{\begin{vmatrix} C_{nea(i+1)i} & C_{neb(i+1)i} \\ C_{nha(i+1)i} & C_{nhb(i+1)i} \end{vmatrix}} \quad (50a)$$

$$b_{n(i+1)} = \frac{\begin{vmatrix} C_{nea(i+1)i} & L_{neii} \\ C_{nha(i+1)i} & L_{nhii} \end{vmatrix}}{\begin{vmatrix} C_{nea(i+1)i} & C_{neb(i+1)i} \\ C_{nha(i+1)i} & C_{nhb(i+1)i} \end{vmatrix}}. \quad (50b)$$

Here, left-hand equation information about the previous inner ith annulus is stored in

$$L_{neii} = a_{ni}C_{neaii} + b_{ni}C_{nebii} \quad (51a)$$

$$L_{nhii} = a_{ni}C^{\phi}_{nhaii} + b_{ni}C^{\phi}_{nhbii}. \quad (51b)$$

The fifth index on the C coefficients represents the outer radius r_{iO} of the inner annulus i or the inner radius $r_{(i+1)I}$ of the outer annulus $(i+1)$.

Formulas (50) can be somewhat simplified by recognizing that the denominators have already been defined in (42). The fifth index A has now been replaced by the subscript i denoting the inner radius $r_{(i+1)I}$ of the outer annulus $(i+1)$ or the outer radius r_{iO} of the inner annulus i. Thus, the fifth index represents the interfacial radius of the last two indices in the new notation and so is a unique specification. Using the more generally constructed determinant

$$D_{i+1} = \begin{vmatrix} C_{nea(i+1)i} & C_{neb(i+1)i} \\ C_{nha(i+1)i} & C_{nhb(i+1)i} \end{vmatrix} \quad (52)$$

the annulus field coefficients $a_{n(i+1)}$ and $b_{n(i+1)}$ look like

$$a_{n(i+1)} = \frac{1}{D_{i+1}}\begin{vmatrix} L_{neii} & C_{neb(i+1)i} \\ L_{nhii} & C_{nhb(i+1)i} \end{vmatrix} \quad (53a)$$

$$b_{n(i+1)} = \frac{1}{D_{i+1}}\begin{vmatrix} C_{nea(i+1)i} & L_{neii} \\ C_{nha(i+1)i} & L_{nhii} \end{vmatrix}. \quad (53b)$$

These expressions implicitly contain forward propagating recursion information from the previous annulus in the L_{neii} and L_{nhii} terms. This information will now be explicitly inserted from (51) into (53), factoring out the previous annulus field coefficients, so that explicit forward propagating recursion formulas result

$$a_{n(i+1)} = \frac{1}{D_{i+1}}\{[C_{nhb(i+1)i}C_{neaii} - C_{neb(i+1)i}C_{nhaii}]a_{ni} + [C_{nhb(i+1)i}C_{nebii} - C_{neb(i+1)i}C_{nhbii}]b_{ni}\} \quad (54a)$$

$$b_{n(i+1)} = \frac{1}{D_{i+1}}\{[C_{nea(i+1)i}C_{nhaii} - C_{nha(i+1)i}C_{neaii}]a_{ni} + [C_{nea(i+1)i}C_{nhbii} - C_{nha(i+1)i}C_{nebii}]b_{ni}\}. \quad (54b)$$

Each term within the square brackets in (54a) and (54b) is a connection term linking the $(i+1)$ and i annuli. Therefore we define them as

$$\alpha_a(i+1,i) = C_{nhb(i+1)i}C_{neaii} - C_{neb(i+1)i}C_{nhaii} \quad (55a)$$

$$\beta_a(i+1,i) = C_{nhb(i+1)i}C_{nebii} - C_{neb(i+1)i}C_{nhbii} \quad (55b)$$

$$\alpha_b(i+1,i) = C_{nea(i+1)i}C_{nhaii} - C_{nha(i+1)i}C_{neaii} \quad (55c)$$

$$\beta_b(i+1,i) = C_{nea(i+1)i}C_{nhbii} - C_{nha(i+1)i}C_{nebii}. \quad (55d)$$

With these assignments, the recursion expressions (54) are

$$a_{n(i+1)} = \frac{1}{D_{i+1}}\{\alpha_a(i+1,i)a_{ni} + \beta_a(i+1,i)b_{ni}\} \quad (56a)$$

$$b_{n(i+1)} = \frac{1}{D_{i+1}}\{\alpha_b(i+1,i)a_{ni} + \beta_b(i+1,i)b_{ni}\}. \quad (56b)$$

Since the coupling terms $\alpha_p(i+1,i)$ and $\beta_p(i+1,i)$, $p = a, b$, can be determined once the material parameters of the different rings are specified and the ring geometries set, the field coefficients of any succeeding ring can be found by (56). Starting from the first annulus $i = 1$, (56) may be successively applied (recursively) until the outermost (last) $i = N$ annulus is reached. The iterative process must be repeated $N-1$ times for N annuli, taking us from the field coefficient information in the innermost first annulus a_{n1} and b_{n1}, to the field coefficient information in the last annulus a_{nN} and b_{nN}.

E. Nth Annulus—Outer Region Boundary Conditions

The progression of annuli may be effectively truncated at the $r = R$ boundary of the device where the last $i = N$ annulus ends and the outer region of the device begins. It is here that ports exit from the device. It is also here that the device transitions from a ferrite medium to a dielectric medium. If one wishes to stop the 2-D field analysis at $r = R$, then approximating boundary conditions must be applied here to model the effect of the ports and the change at the other contour regions where the device becomes dielectric. The first requirement is met by imposing constraints typical of those describing a circulator-microstrip line (or stripline) interface. The second requirement is met by assuming magnetic wall conditions where the device transitions from ferrite to dielectric.

At the perimeter $r = R$, the boundary condition on H_ϕ consistent with both requirements is a Dirichlet boundary

condition (BC)

$$H_\phi^{\rm Per}(R,\phi)=\begin{cases} H_a;\phi_a-\Delta\phi_a/2<\phi<\phi_a+\Delta\phi_a/2 \\ H_b;\phi_b-\Delta\phi_b/2<\phi<\phi_b+\Delta\phi_b/2 \\ H_c;\phi_c-\Delta\phi_c/2<\phi<\phi_c+\Delta\phi_c/2 \\ 0; \quad \text{nonport contour regions.}\end{cases} \tag{57}$$

An arbitrary function like that specified in (57) can be represented by a one-dimensional Fourier series over the appropriate domain $(-\pi,\pi)$

$$H_\phi^{\rm per}(R,\phi)=\sum_{m=-\infty}^{\infty}A_m e^{\imath m\phi}. \tag{58}$$

Multiplying both sides of (58) by $\exp(-in\ \phi)$, integrating over the domain, and using the orthogonality property

$$\int_{-\pi}^{\pi}e^{im\phi}e^{-in\phi}d\phi=\begin{cases}2\pi; & m=n\\ 0; & m\neq n\end{cases} \tag{59}$$

yields the nth coefficient of the expansion

$$A_n=\frac{1}{2\pi}\int_{-\pi}^{\pi}H_\phi^{\rm Per}(R,\phi)e^{-\imath n\phi}d\phi. \tag{60}$$

These coefficients must be precisely the same as those found in the Bessel–Fourier expansion provided for the H_ϕ field solution for the last annulus in (34). Setting $\imath=N$, and $r=R$

$$H_{\phi N}=\sum_{n=-\infty}^{\infty}\left[a_{nN}C^{\phi}_{nhaN}(R)+b_{nN}C^{\phi}_{nhbN}(R)\right]e^{\imath n\phi}. \tag{61}$$

Equating $H_\phi^{\rm Per}(R,\phi)$ and $H_{\phi N}$, and using the orthogonality property of the Fourier harmonic functions, we find that

$$\begin{aligned}A_n&=a_{nN}C^{\phi}_{nhaN}(R)+b_{nN}C^{\phi}_{nhbN}(R)\\ &=a_{nN}C^{\phi}_{nhaNO}+b_{nN}C^{\phi}_{nhbNO}\\ &=a_{nN}C^{\phi}_{nhaNR}+b_{nN}C^{\phi}_{nhbNR}\end{aligned} \tag{62}$$

where the second equality is consistent with earlier convention to attribute the fifth index "O" to the fourth index $i=N$ thereby assigning the radius for argument evaluation of the C coefficient as r_{NO} and where the third equality simply registers explicitly the radius for argument evaluation as $r=R$.

Examination of (44) and the linear mapping process implied by (56) indicates that a_{nN} and b_{nN} can be written as

$$a_{nN}=a_{nN}(\text{recur})a_{n0} \tag{63a}$$

$$b_{nN}=b_{nN}(\text{recur})a_{n0}. \tag{63b}$$

Here $a_{nN}(\text{recur})$ and $b_{nN}(\text{recur})$ denote the quantities obtained by applying forward recursion formulas (56) $N-1$ times starting with the formulas (44) and at the end factoring out the single factors a_{n0} from the final a_{nN} and b_{nN} results. The recipe for getting $a_{nN}(\text{recur})$ and $b_{nN}(\text{recur})$ requires a_{n0} to be formally set to unity in (44) and the recursion process executed as described. Equations (63) are extremely important relations. Inserting them into (62) and solving for a_{n0} gives

$$a_{n0}=\frac{A_n}{a_{nN}(\text{recur})C^{\phi}_{nhaNR}+b_{nN}(\text{recur})C^{\phi}_{nhbNR}}. \tag{64}$$

Because all the quantities are known on the right-hand side of (64), a_{n0} is determined. Once a_{n0} is determined, all the fields in all the annuli are known by the very nature of the recursion process. In this way, the driving or forcing function contained in (57) and implicitly stored in A_n, leads to the fields to be specified. That relationship means that we can now find the Green's functions relating forcing contour field $H_{\phi c}(R,\phi)$ to $E_z(r,\phi)$. Thus, we will be finding the various components of the recursive Green's functions.

III. Recursive Green's Functions

A. Within the Disk

The cross- (or indirect) coupling Green's function relating forcing contour field $H_{\phi c}(R,\phi)$ to $E_z(r,\phi)$ will be found here. First the fields will be examined within the disk, then the fields on the outermost annulus-exterior interface.

Invoking (64), and putting a_{n0} into (27) and (28) gives the three field components at any (r,ϕ) location within the disk

$$E_{z0}(r,\phi)=\sum_{n=-\infty}^{\infty}\frac{A_n}{a_{nN}(\text{recur})C^{\phi}_{nhaNR}+b_{nN}(\text{recur})C^{\phi}_{nhbNR}}\times C_{nea0}(r)e^{\imath n\phi}. \tag{65}$$

To find the Green's function form of solution, the implicit forcing function information in A_n must be made explicit by replacing A_n with (60), properly extracting the forcing field from the integral. Identify $N_{\rm Trp}$ contour regions where $H_\phi^{\rm Per}(R,\phi)$ is nonzero

$$H_\phi^{\rm Per}(R,\phi)=\sum_{q=1}^{N_{\rm Trp}}H_\phi^{\rm Per}(R,\phi_q)\delta(\phi-\phi_q)\Delta\phi_q. \tag{66}$$

Inserting (66) into (60) and reversing the order of summations and integrations gives

$$A_n=\frac{1}{2\pi}\sum_{q=1}^{N_{\rm Trp}}\int_{-\pi}^{\pi}H_\phi^{\rm Per}(R,\phi_q)\delta(\phi-\phi_q)\Delta\phi_q e^{-\imath n\phi}d\phi. \tag{67}$$

Performing the integration gives

$$A_n=\frac{1}{2\pi}\sum_{q=1}^{N_{\rm Trp}}H_\phi^{\rm Per}(R,\phi_q)\Delta\phi_q e^{-in\phi_q}. \tag{68}$$

Returning to (65), and substituting for A_n

$$E_{z0}(r,\phi)=\frac{1}{2\pi}\sum_{n=-\infty}^{\infty}\frac{\sum_{q=1}^{N_{\rm Trp}}H_\phi^{\rm Per}(R,\phi_q)\Delta\phi_q e^{-\imath n\phi_q}}{a_{nN}(\text{recur})C^{\phi}_{nhaNR}+b_{nN}(\text{recur})C^{\phi}_{nhbNR}}\times C_{nea0}(r)e^{\imath n\phi}. \tag{69}$$

Reversing the order of Fourier azimuthal harmonic summation and the port (discretization) summation produces

$$E_{z0}(r,\phi)=\frac{1}{2\pi}\sum_{q=1}^{N_{\rm Trp}}\sum_{n=-\infty}^{\infty}\frac{C_{nea0}(r)}{a_{nN}(\text{recur})C^{\phi}_{nhaNR}+b_{nN}(\text{recur})C^{\phi}_{nhbNR}}\times e^{-\imath n\phi_q}e^{\imath n\phi}H_\phi^{\rm Per}(R,\phi_q)\Delta\phi_q. \tag{70}$$

This can be considerably streamlined by defining the constant denominator term to be

$$\gamma_{nN} = a_{nN}(\text{recur})C^{\phi}_{nhaNR} + b_{nN}(\text{recur})C^{\phi}_{nhbNR} \tag{71}$$

and placing it into (70)

$$E_{z0}(r,\phi) = \frac{1}{2\pi}\sum_{q=1}^{N_{\text{Trp}}}\sum_{n=-\infty}^{\infty}\frac{C_{nea0}(r)}{\gamma_{nN}}e^{-\imath n\phi_q}e^{\imath n\phi}H^{\text{Per}}_{\phi}(R,\phi_q)\Delta\phi_q. \tag{72}$$

From the discussion at the beginning of Section II, we can recognize

$$H_{\phi c}(R,\phi') = H^{\text{Per}}_{\phi}(R,\phi_q) \tag{73}$$

and perform the limiting process

$$\text{limit } \Delta\phi_q \to 0. \tag{74}$$

When these two activities are completed, the $z\phi$ cross-coupling Green's function element arises from (72) as

$$G^{z\phi}_{\text{EH}}(r,\phi;R,\phi_q) = \frac{1}{2\pi}\sum_{n=-\infty}^{\infty}\frac{C_{nea0}(r)}{\gamma_{nN}}e^{-\imath n\phi_q}e^{\imath n\phi}. \tag{75}$$

The electric field $E_{z0}(r.\phi)$ is obtained from (75) by multiplying the Green's function by $H^{\text{Per}}_{\phi}(R,\phi_q)$ then applying to this product the discretization operator obtained from the integral operator by the assignment

$$\int_{-\pi}^{\pi}[\,]d\phi \to \sum_{q=1}^{N_{\text{Trp}}}[\,]\Delta\phi_q. \tag{76}$$

That is, (4) in integral form

$$E_{z0}(r,\phi) = \int_{-\pi}^{\pi}G^{z\phi}_{\text{EH}}(r,\phi;R,\phi')H_{\phi c}(R,\phi')d\phi' \tag{77}$$

now reads in discretized form

$$E_{z0}(r,\phi) = \sum_{q=1}^{N_{\text{Trp}}}G^{z\phi}_{\text{EH}}(r,\phi;R,\phi_q)H_{\phi c}(R,\phi_q)\Delta\phi_q. \tag{78}$$

It may be desirable to consider the case where the forcing contour field $H_{\phi c}(R,\phi)$ is treated as constant over some regions. Therefore we will consider N^c_{Trp} port regions where $H_{\phi c}(R,\phi)$ can be removed from the integrations in (77). This will require a generalization of the integral-to-discretization operator mapping provided in (76)

$$\int_{-\pi}[\,]d\phi \to \sum_{q=1}^{N^d_{\text{Trp}}}[\,]\Delta\phi_q + \sum_{v=1}^{N^c_{\text{Trp}}}\int_{\phi_v-\Delta\phi_v/2}^{\phi_v+\Delta\phi_v/2}[\,]d\phi. \tag{79}$$

There are now a total of N_{Trp} port regions, some of which are discretized into elements and some of which are continuously treated

$$N_{\text{Trp}} = N^d_{\text{Trp}} + N^c_{\text{Trp}}. \tag{80}$$

Equation (78) becomes

$$E_{z0}(r,\phi) = \sum_{q=1}^{N^d_{\text{Trp}}}G^{z\phi}_{\text{EH}}(r,\phi;R,\phi_q)H_{\phi c}(R,\phi_q)\Delta\phi_q + \sum_{v=1}^{N^c_{\text{Trp}}}H_{\phi c}(R,\phi_v)\int_{\phi_v-\Delta\phi_v/2}^{\phi_v+\Delta\phi_v/2}G^{z\phi}_{\text{EH}}(r,\phi;R,\phi')d\phi'. \tag{81a}$$

Our choice will be to let $N^d_{\text{Trp}} \geq 1$ and $N^c_{\text{Trp}} = 0$ or $N^d_{\text{Trp}} = 0$ and $N^c_{\text{Trp}} \geq 1$ noting that the null value indicates that no sum occurs [26]. The first selection allows for infinitesimal ports and the second continuous ports. Therefore, we find for the continuous port case that

$$E_{z0}(r,\phi) = \sum_{v=1}^{N^c_{\text{Trp}}}\bar{G}^{z\phi}_{\text{EH}}(r,\phi;R,\phi_v)H_{\phi c}(R,\phi_v)\Delta\phi_v \tag{81b}$$

defining a modified Green's function

$$\bar{G}^{z\phi}_{\text{EH}}(r,\phi;R,\phi_v) = \frac{1}{2\pi}\sum_{n=-\infty}^{\infty}\frac{C_{nea0}(r)}{\gamma_{nN}}\bar{I}^v_n e^{\imath n\phi}. \tag{82}$$

For the continuous port the expression was made to look like the discretized port expression by defining a modified definite integral which is normalized to the finite angular width of the port region $\Delta\phi_v$

$$\bar{I}^v_n = \frac{I^v_n}{\Delta\phi_v} \tag{83}$$

where the definite integral evaluation is

$$I^v_n = \int_{\phi_v-\Delta\phi_v/2}^{\phi_v+\Delta\phi_v/2}e^{-\imath n\phi'}d\phi' = \frac{2}{n}\sin\left(n\frac{\Delta\phi_v}{2}\right)e^{-in\phi_v}. \tag{84}$$

B. On the Outer Annulus-Port Interface

Due to the separable nature of the governing equation (16), and the resulting sourceless solution being the product of radial and azimuthal functions, the Green's function evaluated on the contour $r = R$ simplifies significantly. The Green's function and the fields found as a result are of importance in relating the solution found inside the ferrite circulator domain on $0 \leq r \leq R$ and $-\pi \leq \phi \leq \pi$ to the outside structure, namely the interfacing ports.

If we assign a notation similar to that found in (71) to the radial numerator factor, developed from (31) with $i = N$

$$\gamma^{\text{ze}}_{nN} = a_{nN}(\text{recur})C_{neaN}(R) + b_{nN}(\text{recur})C_{nebN}(R) \tag{85}$$

with upgraded notation being employed here. Furthermore, let us define normalized quantities

$$\bar{\gamma}^{pq}_{nN} = \frac{\gamma^{pq}_{nN}}{\gamma^{\phi h}_{nN}}. \tag{86}$$

Here, $p = z, r$, or ϕ; $q = e$ or h.

With the definitions (85) and (86), the field and recursive Green's function can be stated as

$$E_{zN}(R,\phi) = \sum_{q=1}^{N_{\mathrm{Trp}}^{d}} G_{\mathrm{EHN}}^{z\phi}(R,\phi;R,\phi_q)H_{\phi c}(R,\phi_q)\Delta\phi_q + \sum_{v=1}^{N_{\mathrm{Trp}}^{c}} \bar{G}_{\mathrm{EHN}}^{z\phi}(R,\phi;R,\phi_v)H_{\phi c}(R,\phi_v)\Delta\phi_v \quad (87)$$

where

$$G_{\mathrm{EHN}}^{z\phi}(R,\phi;R,\phi_q) = \frac{1}{2\pi}\sum_{n=-\infty}^{\infty} \bar{\gamma}_{nN}^{z\phi} e^{-in\phi_q} e^{in\phi} \quad (88)$$

and the modified expression

$$\bar{G}_{\mathrm{EHN}}^{z\phi}(R,\phi;R,\phi_v) = \frac{1}{2\pi}\sum_{n=-\infty}^{\infty} \bar{\gamma}_{nN}^{z\phi}\bar{I}_n^v e^{in\phi}. \quad (89)$$

IV. Scattering Parameters for a Three-Port Circulator

Here we will consider a particularly simple case where the circulator either has discretized ports (actually very small as to appear infinitesimal) or continuous ports but not both. Furthermore, if discretized ports are treated, then only one element per port is allowed. In effect, what that means is that the angular extent of the ports is considered so small that a single element is sufficient to approximate the port contour. The general case for many elements is treated elsewhere [26]. Thus, (87) becomes, if we limit the device to three ports, making $N_{\mathrm{Trp}}^{d} = N_{\mathrm{Trp}}^{c} = 3$

$$E_{zN}(R,\phi) = \sum_{q=1}^{3} \tilde{G}_{\mathrm{EHN}}^{z\phi}(R,\phi;R,\phi_q) \times H_{\phi c}(R,\phi_q)\Delta\phi_q \quad (90)$$

where

$$\tilde{G}_{\mathrm{EHN}}^{z\phi}(R,\phi;R,\phi_q) = \begin{cases} G_{\mathrm{EHN}}^{z\phi}(R,\phi;R,\phi_q); & \text{discretized} \\ \bar{G}_{\mathrm{EHN}}^{z\phi}(R,\phi;R,\phi_q); & \text{continuous.} \end{cases} \quad (91)$$

If we absorb the azimuthal spread into the Green's function by defining a modified form

$$\tilde{\tilde{G}}(\phi;\phi_q) = \tilde{G}_{\mathrm{EHN}}^{z\phi}(R,\phi;R,\phi_q)\Delta\phi_q \quad (92)$$

where the understood indices and arguments have been dropped, (90) can be expanded as

$$E_{zN}(R,\phi) = \tilde{\tilde{G}}(\phi,\phi_a)H_a + \tilde{\tilde{G}}(\phi,\phi_b)H_b + \tilde{\tilde{G}}(\phi;\phi_c)H_c. \quad (93)$$

Now evaluate (93) at each of the ports, $q = a, b, c$, labeled counterclockwise, and simplify the notation for $E_{zN}(R,\phi)$ to E_z^q by setting $\phi = \phi_q$

$$E_z^a = \tilde{\tilde{G}}(\phi_a,\phi_a)H_a + \tilde{\tilde{G}}(\phi_a,\phi_b)H_b + \tilde{\tilde{G}}(\phi_a,\phi_c)H_c \quad (94a)$$

$$E_z^b = \tilde{\tilde{G}}(\phi_b,\phi_a)H_a + \tilde{\tilde{G}}(\phi_b,\phi_b)H_b + \tilde{\tilde{G}}(\phi_b,\phi_c)H_c \quad (94b)$$

$$E_z^c = \tilde{\tilde{G}}(\phi_c,\phi_a)H_a + \tilde{\tilde{G}}(\phi_c,\phi_b)H_b + \tilde{\tilde{G}}(\phi_c,\phi_c)H_c. \quad (94c)$$

Let us make a number of practical assumptions which will further simplify the coming analysis. Assume that the input port a is subject to reflections from the transmission line-circulator interface. Therefore s_{11} is nonzero and the match is imperfect for port a. But assume that the other two ports, the output port b and the isolated port c, are perfectly matched to the transmission lines. These assumptions translate into the relationships

$$E_{z(\mathrm{in})}^a \neq E_z^a; \quad (95a)$$

$$H_{\phi(\mathrm{in})}^a \neq H_\phi^a, \quad (95b)$$

$$E_{z(\mathrm{out})}^b = E_z^b; \quad (96a)$$

$$H_{\phi(\mathrm{out})}^b = H_\phi^b, \quad (96b)$$

$$E_{z(\mathrm{out})}^c = E_z^c; \quad (97a)$$

$$H_{\phi(\mathrm{out})}^c = H_\phi^c \quad (97b)$$

where the subscript indicates an inward or outward propagating wave along the transmission line in relation to the circulator. Each transmission line is characterized by a wave impedance. Consequently

$$\frac{E_{z(\mathrm{in})}^a}{H_{a(\mathrm{in})}} = \zeta_a \quad (98a)$$

$$\frac{E_{z(\mathrm{out})}^b}{H_{b(\mathrm{out})}} = -\zeta_b \quad (98b)$$

$$\frac{E_{z(\mathrm{out})}^c}{H_{c(\mathrm{out})}} = -\zeta_c. \quad (98c)$$

Next, we define the s-parameters which are to be determined by this process of analysis

$$E_z^a = (1+s_{11})E_{z(\mathrm{in})}^a \quad (99a)$$

$$H_\phi^a = (1-s_{11})H_{\phi(\mathrm{in})}^a \quad (99b)$$

$$s_{21} = \frac{E_{z(\mathrm{out})}^b}{E_{z(\mathrm{in})}^a} \quad (100)$$

$$s_{31} = \frac{E_{z(\mathrm{out})}^c}{E_{z(\mathrm{in})}^a}. \quad (101)$$

These last formulas (95)–(99) must be combined to utilize only the total fields in the transmission lines because at the circulator-transmission line interfaces we relate the z and ϕ components by interfacial tangential boundary conditions

$$E_z^q(\mathrm{cir}) = E_z^q(\mathrm{TL}); \quad (102a)$$

$$H_\phi^q(\mathrm{cir}) = H_\phi^q(\mathrm{TL}) \quad (102b)$$

where formulas (102) relate total fields. When this is done

$$E_z^a = \frac{1+s_{11}}{1-s_{11}}\zeta_a H_a \quad (103a)$$

$$s_{21} = (1+s_{11})\frac{E_z^b}{E_z^a} \quad (103b)$$

$$s_{31} = (1+s_{11})\frac{E_z^c}{E_z^a} \quad (103c)$$

$$\frac{E_z^b}{H_b} = -\zeta_b \quad (104a)$$

$$\frac{E_z^c}{H_c} = -\zeta_c. \quad (104b)$$

Make the input field $E^a_{z(in)} = 1$ and put it into (99a) so that the H-field is determined in terms of the input s-parameter in (103a). We obtain

$$E^a_z = (1 + s_{11}) \tag{105}$$

$$\frac{\zeta_a H_a}{1 - s_{11}} = 1. \tag{106}$$

Combining these two equations eliminates s_{11}

$$E^a_z = 2 - \zeta_a H_a. \tag{107}$$

Now using (104) and (107), remove the E-field unknowns from (94), obtaining a simultaneous set of three equations in three unknown H-fields

$$2 - \zeta_a H_a = G_{aa}H_a + G_{ab}H_b + G_{ac}H_c \tag{108a}$$

$$-\zeta_b H_b = G_{ba}H_a + G_{bb}H_b + G_{bc}H_c \tag{108b}$$

$$-\zeta_c H_c = G_{ca}H_a + G_{cb}H_b + G_{cc}H_c \tag{108c}$$

Rewriting (108)

$$(G_{aa} + \zeta_a)H_a + G_{ab}H_b + G_{ac}H_c = 2 \tag{109a}$$

$$G_{ba}H_a + (G_{bb} + \zeta_b)H_b + G_{bc}H_c = 0 \tag{109b}$$

$$G_{ca}H_a + G_{cb}H_b + (G_{cc} + \zeta_c)H_c = 0. \tag{109c}$$

The solution for the H-fields is

$$H_a = \frac{1}{D_p}\begin{vmatrix} 2 & G_{ab} & G_{ac} \\ 0 & (G_{bb} + \zeta_b) & G_{bc} \\ 0 & G_{cb} & (G_{cc} + \zeta_c) \end{vmatrix}$$

$$= \frac{2}{D_p}[(G_{bb} + \zeta_b)(G_{cc} + \zeta_c) - G_{bc}G_{cb}] \tag{110a}$$

$$H_b = \frac{1}{D_p}\begin{vmatrix} (G_{aa} + \zeta_a) & 2 & G_{ac} \\ G_{ba} & 0 & G_{bc} \\ G_{ca} & 0 & (G_{cc} + \zeta_c) \end{vmatrix}$$

$$= -\frac{2}{D_p}[G_{ba}(G_{cc} + \zeta_c) - G_{bc}G_{ca}] \tag{110b}$$

$$H_c = \frac{1}{D_p}\begin{vmatrix} (G_{aa} + \zeta_a) & G_{ab} & 2 \\ G_{ba} & (G_{bb} + \zeta_b) & 0 \\ G_{ca} & G_{cb} & 0 \end{vmatrix}$$

$$= \frac{2}{D_p}[G_{ba}G_{cb} - (G_{bb} + \zeta_b)G_{ca}] \tag{110c}$$

where the H-field system determinant is

$$D_p = \begin{vmatrix} (G_{aa} + \zeta_a) & G_{ab} & G_{ac} \\ G_{ba} & (G_{bb} + \zeta_b) & G_{bc} \\ G_{ca} & G_{cb} & (G_{cc} + \zeta_c) \end{vmatrix}. \tag{111}$$

The H-fields have been found and from them the s-parameters can be obtained also. Equation (106) gives

$$s_{11} = 1 - \zeta_a H_a \tag{112a}$$

$$s_{21} = E^b_z = -\zeta_b H_b \tag{112b}$$

$$s_{31} = E^c_z = -\zeta_c H_c \tag{112c}$$

where the latter two formulas came from using (104) and (105) in (103b) and (103c). Obviously, the E-fields have been obtained by this process too.

V. Contributions to Permeability Tensor and Dielectric Constant

The work here treats radial variation of the ferrite material parameters in circularly shaped stripline or microstrip circulators. The "circular" case is important not only because it is easier to solve than most other shapes, but also because nearly all quasi-TEM microwave circulators made today use round ferrite pucks. It is suspected that wider bandwidth circulators can result from the use of multiple ferrite material rings [27] and possibly from bias field shaping.

Fig. 1 shows a circulator with a central disk (region 0) and four annuli (regions 1–4). Each region shown in Fig. 1 may represent a different ferrite material; or it may simply represent a computational region in which the material is the same as its neighbors but the demagnetizing factor and/or the applied bias field is different from its neighbors. In either case, the variation of any or all of these three elements (ferrite material type, applied field, and demagnetizing factor) is mathematically lumped into the permeability tensor, (12), in Section II. Also, any radial variation of the dielectric constant and loss tangent with varying ferrite materials is mathematically lumped into the effective propagation constant, (17), in Section II, by way of the complex dielectric constant.

In anisotropic ferromagnetic materials, a relative permeability different from unity arises from the tensor magnetic susceptibility, $\hat{\chi}$, of the material, which relates the H-fields to the magnetization, $\boldsymbol{M} = \hat{\chi}\boldsymbol{H}$. The relative permeability, which relates B-fields to H-fields, $\boldsymbol{B} = \hat{\mu}\boldsymbol{H}$, is

$$\hat{\mu} = \hat{1} + \hat{\chi} = \begin{bmatrix} 1 & 0 & 0 \\ 0 & 1 & 0 \\ 0 & 0 & 1 \end{bmatrix} + \begin{bmatrix} \chi_{xx} & -i\chi_{xy} & 0 \\ i\chi_{yx} & \chi_{yy} & 0 \\ 0 & 0 & 0 \end{bmatrix}$$

$$= \begin{bmatrix} 1 + \chi_{xx} & -i\chi_{xy} & 0 \\ i\chi_{yx} & 1 + \chi_{yy} & 0 \\ 0 & 0 & 1 \end{bmatrix}$$

$$= \begin{bmatrix} \mu & -i\kappa & 0 \\ i\kappa & \mu & 0 \\ 0 & 0 & 1 \end{bmatrix}. \tag{113}$$

The susceptibility terms are complex. The complex $\mu = \mu' - j\mu''$ and $\kappa = \kappa' - j\kappa''$ are rf permeability terms and the unity term is the DC permeability affecting the bias field, where in rectangular coordinates the bias field is in the z-direction. Expressions for the real and imaginary parts of μ and κ are conveniently developed from [28] and (113)

$$\mu' = 1 + \frac{\omega_m\omega_0[\omega_0^2 - \omega^2(1 - \alpha_m^2)]}{[\omega_0^2 - \omega^2(1 + \alpha_m^2)]^2 + 4\omega^2\omega_0^2\alpha_m^2}$$

$$\mu'' = \frac{\omega_m\omega\alpha_m[\omega_0^2 + \omega^2(1 + \alpha_m^2)]}{[\omega_0^2 - \omega^2(1 + \alpha_m^2)]^2 + 4\omega^2\omega_0^2\alpha_m^2}$$

$$\kappa' = \frac{-\omega_m\omega[\omega_0^2 - \omega^2(1 + \alpha_m^2)]}{[\omega_0^2 - \omega^2(1 + \alpha_m^2)]^2 + 4\omega^2\omega_0^2\alpha_m^2} \tag{114}$$

$$\kappa'' = \frac{-2\omega_m\omega_0\omega^2\alpha_m}{[\omega_0^2 - \omega^2(1 + \alpha_m^2)]^2 + 4\omega^2\omega_0^2\alpha_m^2}.$$

In these expressions $\omega_m = -\gamma M \approx -\gamma M_s$ in which M_s is the saturation magnetization, $\omega_0 = -\gamma H_i$ in which H_i is the internal bias field, ω is the actual operating radian frequency, and

α_m is the damping term, related to magnetic linewidth ΔH by $\alpha_m = -\Delta H\gamma/2\omega$, and γ is the gyromagnetic ratio whose value in MKS units is -2.2126×10^5 (rad/s)/(ampturns/m). Also, the internal bias field is equal to the external applied field, $H_{\rm app}$, minus the product of the demagnetizing factor, $N_d = N_{zz}$, and the saturation magnetization, M_s, giving $H_i = H_{\rm app} - N_{zz}M_s$ when written in the format consistent with MKS-unit thinking. In this equation, M and H are both in ampturns/m. N_{zz} describes the z component of the demagnetizing field when the sample is magnetized in the z direction. For those more familiar with Gaussian-unit thinking, this equation would read $H_i = H_{\rm app} - N_{zz}4\pi M_s$, where $4\pi M_s$ is in Gauss and H is in Oersteds. N_{zz} varies from point-to-point in the ferrite puck and has a value between zero and one. A first-order estimate of the magnitude and shape of N_{zz} in a uniform circular ferrite puck is given in [29]. In practice, $|H_{\rm app}| > N_{zz} * 4\pi M_s$ must be maintained at all points in all the ferrite material rings; this is because the initial assumption in the derivation of the equation of motion of the total magnetization $\mathbf{M} = \hat{z}M_s + \mathbf{m}e^{i\omega t}$, in the presence of a small rf magnetization $\mathbf{m}$, is that the material be saturated. This implies a steady-state, z-directed magnetization M_z equal to the saturation magnetization M_s, created by an internal bias field in the same direction at all points.

In summary, the basic terms which can vary from point-to-point (or ring-to-ring for the case here) are M_s, $H_{\rm app}$, N_{zz}, and ΔH, accounted for in the permeability tensor; and the ferrite dielectric constant and loss tangent, accounted for in the complex dielectric constant. An additional constraint is $H_i > 0$ everywhere in the ferrite material.

VI. Numerical Results

The information in Sections II, III, and IV has been used to create a computer code for calculating the performance of three-port microstrip and stripline circulators. It is not obvious from a cursory comparison of the mathematical expressions here and those in Bosma [18], [19], but the expressions here reduce exactly to the Bosma result for the radially uniform case. In (89) above, the Green's function consists of three factors: $e^{in\phi}$ which is related to a specific E_z location, $\bar{I}_n^v$ which is related to a specific perimeter H_ϕ location and port angle, and $\bar{\gamma}_{nN}^{z\phi}$. The product $\bar{I}_n^v e^{in\phi}$ involves the perimeter boundary and is the same for either a uniform circulator puck (as in Bosma) or one with radial variations. Therefore, to determine analytical equivalence, it is only necessary to show that the solution of $\bar{\gamma}_{nN}^{z\phi}$ for a single region be the same as that part of the Bosma solution. By using an inner disk of radius r_0 and one outer annulus of outside radius r_1, and then setting $r_1 = r_0$, with the material parameters of the outer annulus the same as those of the inner disk, the case of a uniform puck can be derived. From (86) above, for one annulus

$$\begin{aligned}
\bar{\gamma}_{n1} &= \frac{\gamma_{n1}}{\gamma'_{n1}} \\
\gamma_{n1} &= a_{n1}(\text{recur})C_{nea1O} + b_{n1}(\text{recur})C_{neb1O} \\
\gamma'_{n1} &= a_{n1}(\text{recur})C'_{nha1O} + b_{n1}(\text{recur})C_{nhb1O}
\end{aligned}$$

$$\begin{aligned}
a_{n1}(\text{recur}) &= \frac{M_{01}}{D_1} = \frac{\begin{vmatrix} C_{nea0O} & C_{neb1I} \\ C_{nha0O} & C_{nhb1I} \end{vmatrix}}{\begin{vmatrix} C_{nea1I} & C_{neb1I} \\ C_{nha1I} & C_{nhb1I} \end{vmatrix}} \\
b_{n1}(\text{recur}) &= \frac{M_{02}}{D_1} = \frac{\begin{vmatrix} C_{nea1I} & C_{nea0O} \\ C_{nha1I} & C_{nha0O} \end{vmatrix}}{\begin{vmatrix} C_{nea1I} & C_{neb1I} \\ C_{nha1I} & C_{nhb1I} \end{vmatrix}}.
\end{aligned} \tag{115}$$

In these expressions, the following relationships apply. They are written out to help clarify the subscript meanings

$$\begin{aligned}
C_{nea1O} &= J_n(k_{\text{eff},1}r_1) \\
C_{neb1O} &= N_n(k_{\text{eff},1}r_1) \\
C_{nha1O} &= c_1\left[k_{\text{eff},1}J'_n(k_{\text{eff},1}r_1) - \frac{n\kappa_1}{\mu_1 r_1}J_n(k_{\text{eff},1}r_1)\right] \\
C_{nhb1O} &= c_1\left[k_{\text{eff},1}N'_n(k_{\text{eff},1}r_1) - \frac{n\kappa_1}{\mu_1 r_1}N_n(k_{\text{eff},1}r_1)\right] \\
C_{nea0O} &= J_n(k_{\text{eff},0}r_0) \\
C_{neb1I} &= N_n(k_{\text{eff},1}r_0) \\
C_{nea1I} &= J_n(k_{\text{eff},1}r_0) \\
C_{nha0O} &= c_0\left[k_{\text{eff},0}J'_n(k_{\text{eff},0}r_0) - \frac{n\kappa_0}{\mu_{i=0}r_0}J_n(k_{\text{eff},0}r_0)\right] \\
C_{nhb1I} &= c_1\left[k_{\text{eff},1}N'_n(k_{\text{eff},1}r_0) - \frac{n\kappa_1}{\mu_1 r_1}N_n(k_{\text{eff},1}r_0)\right] \\
C_{nha1I} &= c_1\left[k_{\text{eff},1}J'_n(k_{\text{eff},1}r_0) - \frac{n\kappa_1}{\mu_1 r_0}J_n(k_{\text{eff},1}r_0)\right] \\
c_m &= \frac{i}{\omega\mu_0\mu_{\text{eff},m}}.
\end{aligned} \tag{116}$$

For the special case of $r_1 = r_0 = r$, $k_{\text{eff},1} = k_{\text{eff},0} = k_{\text{eff}}$, $c_1 = c_0 = c$, and using $x = k_{\text{eff}}r$, then $M_{02} = 0$. Also, M_{01} contains the product of the Wronskian (discussed in [30])

$$\begin{aligned}
W\{J_n(x), N_n(x)\} &= J_n(x)N'_n(x) - N_n(x)J'_n(x) \\
&= 2/(\pi x)
\end{aligned}$$

and a nonzero constant, so that

$$\bar{\gamma}_{n1} = \frac{i\omega\mu_0\mu_{\text{eff}}}{k_{\text{eff}}}\frac{J_n(x)}{\left[J'_n(x) - \frac{n\kappa}{\mu x}J_n(x)\right]}. \tag{117}$$

Using Bosma's effective wave impedance, $\zeta_{\text{eff}} = \omega\mu_0\mu_{\text{eff}}/k_{\text{eff}}$, $\bar{\gamma}_{n1}$ becomes

$$\bar{\gamma}_{n1} = i\zeta_{\text{eff}}\frac{J_n(x)}{\left[J'_n(x) - \frac{n\kappa}{\mu x}J_n(x)\right]}. \tag{118}$$

This is exactly the equivalent part of the Bosma [18] double-sided summation expression (60) which leads directly to the single-sided summation in his expression (61).

The code here has been tested for a circulator with a single region of ferrite material and for a multiregion circulator in which the ferrite materials are all alike. The computed results were identical when the material, bias field, demagnetizing

conditions, and outer radius were the same for the two cases. Also the new code gave computed results on uniform cases which were exactly the same as those given by a code developed earlier at NRL [6], [7], based on [18], [19], which was only for radially uniform cases. The validity of the earlier NRL code has been put on firm ground with good comparisons with other calculated results and with experimental data [6], [7], so the new code is equally valid.

The exact agreement between the Bosma approach and that described here requires the use of the same definition for E_z at the circulator ports in the two approaches. Bosma derived and used an expression for the average electric field in [19] for a strip transmission line, while the derivation here uses the field at the center of the strip, whether stripline or microstrip. The difference between the two is that, in (84) above, an additional multiplying term of

$$\sin\left(n\frac{\Delta\phi_v}{2}\right)\Big/\left(n\frac{\Delta\phi_v}{2}\right) \tag{119}$$

appears in the Bosma result for $\bar{I}_n^v$ when average E_z field is used, which then appears in the summation of terms in the recursive Green's function in (82). The difference between the two in the final calculated performance is not great, but, for exact agreement with Bosma's original intention (119), must be incorporated. It is not known at this time whether the use of average field or center field gives better agreement with laboratory measured results. The numerical results which follow were based on the use of the center value of E_z at the ports. The microstrip circulator used for the reference numerical calculations is described in Fig. 2. There is a single quarter-wavelength matching transformer included in the calculations.

In the following figures, the reference calculated performance shown in Fig. 3 is with uniform ferrite material, with $N_{zz} = 1$ throughout, and with uniform external applied field of 1780 Oe. Fig. 4 gives the calculated performance when N_{zz} has the values calculated from [29], and shown in Fig. 5, with other parameters unchanged. This curve was approximated using five rings with five values of N_{zz}, averaged in each ring. Fig. 6 gives the calculated performance when the external applied field is allowed to vary as shown in Fig. 7. Again a five-ring approximation was used, with other parameters the same as for the reference case in each ring. Fig. 8 gives the calculated performance when two different ferrite material rings are used, with the inner ring having half the radius of the outer ring. Multiple-ferrite-ring circulators are of interest, in general, because of their potential for wide bandwidth, as suggested in [31]. The inner ring is Trans-Tech G-113 yttrium iron garnet, described in Fig. 2, and the outer ring is Trans-Tech G-500 yttrium-gadolinium-aluminum iron garnet. The pertinent characteristics of the G-500 are: $4\pi M_s = 550$ G, Linewidth = 65 Oe, Dielectric Constant = 14.4, and Loss Tan = 0.0002, and all of these values were used in the outer ring. Although the radial variations cause changes in the circulator performance, it is interesting to see that major deterioration does not occur for the fairly realistic cases studied here. These results, however, should not be extrapolated very far. Applications vary so widely that these results may not be at all like what happens at much higher or lower frequencies and at much wider or narrower bandwidths.

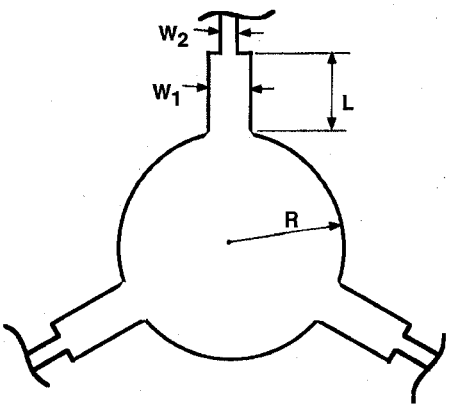

Fig. 2. Top view of the circulator used in the calculations. It has a quarter wave transformer at each port, with $w_1 = 0.096$ cm and $L = 0.241$ cm. Other values are $w_2 = 0.030$ cm for 50 ohm lines and outside radius of magnetized puck is $R = 0.279$ cm. The substrate is a Trans-Tech G113 with a $4\pi M_s = 1780$ G, $\Delta H = 45$ Oe, $\varepsilon_r = 15.0$, and $\tan\delta = 0.0002$. Substrate thickness $H = 0.051$ cm, and conductor thickness = 0.0005 cm.

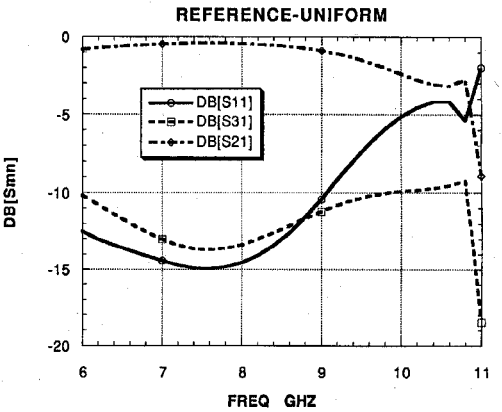

Fig. 3. S-parameters s_{11} (input), s_{31} (isolated) and s_{21} (output) for frequency $f = 6$–11 GHz. These calculated s-parameters for a uniform material distribution will act as reference values for the following figures.

The time required for a single frequency calculation, for $n = -9$ to $+9$ in (89), is shown in Fig. 9. In [7] there is some discussion about the choice of n, but 9 is at the upper limit of the values typically used and, therefore, at the upper limit of calculation time. The Macintosh Quadra 650 results are of the same order as for a 486-type desktop computer. Work station environment is considerably faster. The single-region calculation is handled slightly differently from those for two or more regions, which explains its deviation from the rest of the curve.

VII. Conclusion

With the work presented here it is now possible to obtain information quickly, easily, and inexpensively about the effects of nonuniform demagnetizing factor or bias field, and bandwidth effects of using multiple ferrite rings of different

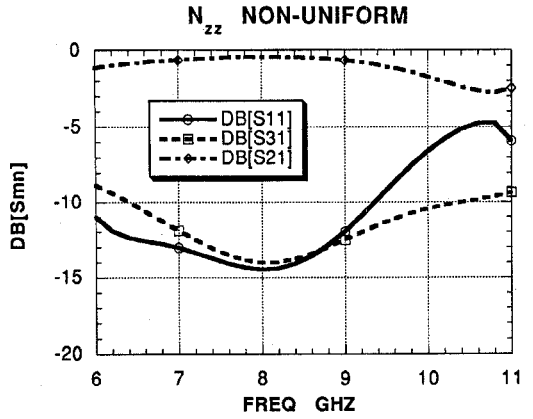

Fig. 4. S-parameters calculated for nonuniform N_{zz} but with other geometric and physical parameters unchanged from Fig. 3. The nonuniform N_{zz} distribution is given in Fig. 5.

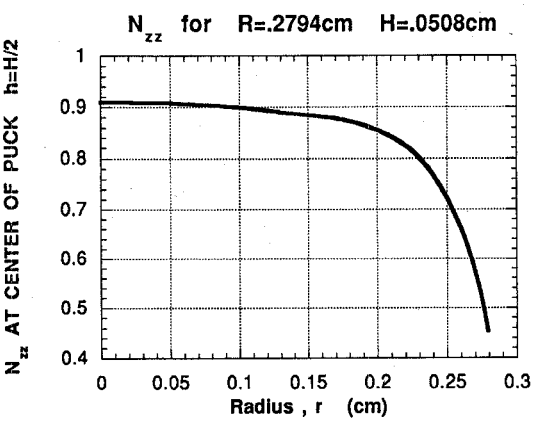

Fig. 5. Variation of N_{zz} in the radial direction, used to generate Fig. 4.

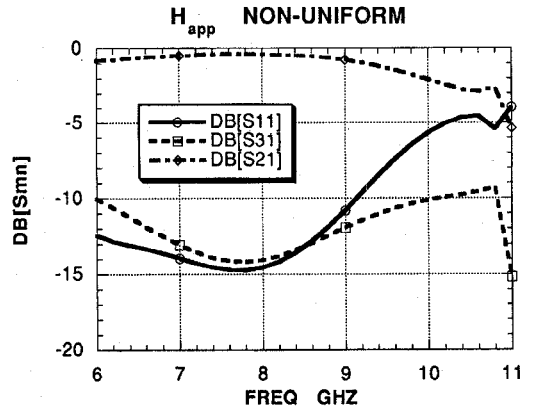

Fig. 6. S-parameters calculated for a nonuniformly applied external $H_{\rm app}$ field.

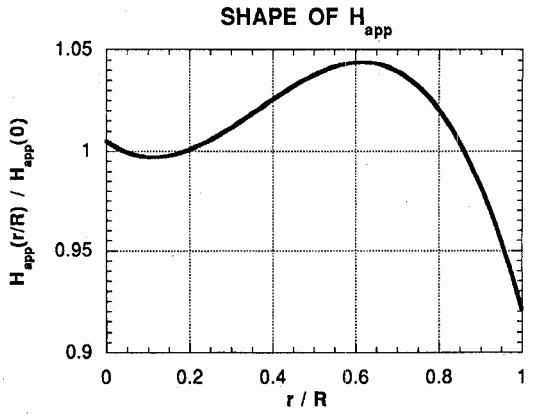

Fig. 7. Variation of $H_{\rm app}$ in the radial direction, used to generate Fig. 6.

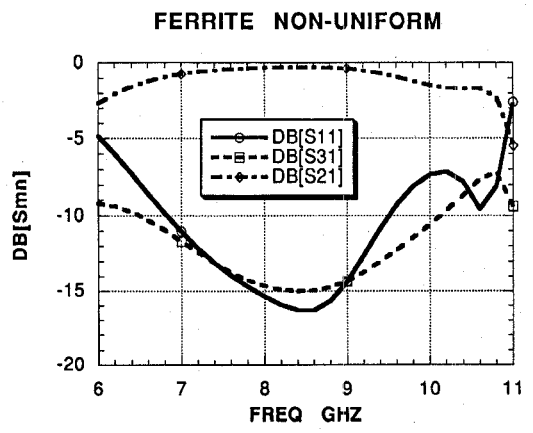

Fig. 8. S-parameters calculated for nonuniform $4\pi M_s = 1780$ G (inner disk), 550 G (annulus). Inner disk material is Trans-Tech G-113 yttrium iron garnet, and outer annulus material is G-500 yttrium gadolinium aluminum iron garnet with $\Delta H = 65$ Oe, $\varepsilon_r = 14.4$, $\tan\delta = 0.0002$.

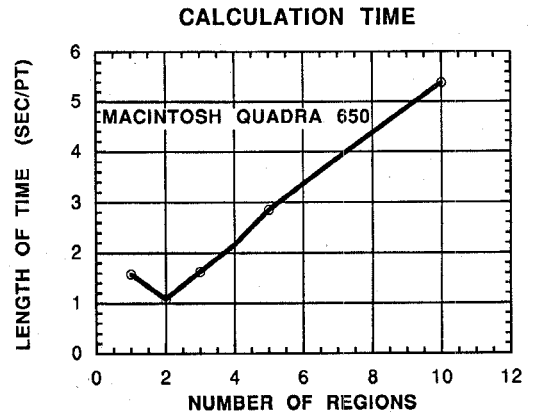

Fig. 9. Computation time of recursive calculation on a MacIntosh Quadra 650 against the number of regions. The inner disk is counted as the first region, with outlying annuli added afterward.

materials. It is a major advantage that only a modest computer platform is required to get these answers.

Here we developed a 2-D recursive Green's function with elements suitable for determining the electric field component E_z anywhere within the circulator. The problem was inhomogeneous because of variations in the applied magnetic field $H_{\rm app}$, magnetization $4\pi M_s$, and demagnetization factor N_d. All magnetic inhomogeneity effects can be put into the frequency dependent tensor elements of the anisotropic permeability tensor $\hat{\mu}$. The recursive nature of the Green's function is a reflection of the inhomogeneous region being broken up into one inner disk containing a singularity and N annuli. Ports were separated into discretized ports with elements or continuous ports located at arbitrary azimuthal ϕ and arbitrary line widths. From the Green's function, s-parameters were found for a simple case of a three-port ferrite circulator. Numerical results have been presented for the case of symmetrically disposed ports of equal widths, taking into account the radial

inhomogeneities. Studies of breaking up the area into 1, 2, and 5 annuli were undertaken to treat specific inhomogeneous problems. A computer code which evaluates the recursive Green's function was shown to be very efficient and to have no convergence problems.

REFERENCES

[1] K. M. Gaukel and E. B. El-Sharawy, "Three-port disk circulator analysis using only port segmentation," in *IEEE MTT-S Int. Microwave Symp. Dig.*, May 1994, pp. 925–927.

[2] L. E. Davis and R. Sloan, "Semiconductor junction circulators," in *IEEE MTT-S Int. Microwave Symp. Dig.*, June 1993, pp. 483–486.

[3] J. Helszajn and D. S. James, "Planar triangular resonators with magnetic walls," *IEEE Trans. Microwave Theory Tech.*, vol. MTT-26, no. 2, pp. 95–100, Feb. 1978.

[4] J. Helszajn and D. J. Lynch, "Cut-off space of cloverleaf resonators with electric and magnetic walls," *IEEE Trans. Microwave Theory Tech.*, vol. 40, no. 8, pp. 1620–1629, Aug. 1992.

[5] R. W. Lyon and J. Helszajn, "A finite element analysis of planar circulators using arbitrarily shaped resonators," *IEEE Microwave Theory Tech.*, vol. MTT-11, no. 11, pp. 1964–1974, Nov. 1982.

[6] R. E. Neidert, "Computer program CIRCREN for Y-junction stripline and microstrip ferrite circulators," *NRL Report 9381*, Apr. 1992.

[7] R. E. Neidert and P. M. Phillips, "Losses in Y-junction stripline and microstrip ferrite circulators," *IEEE Trans. Microwave Theory Tech.*, vol. 41, no. 6/7, pp. 1081–1086, June/July 1993.

[8] T. Miyoshi and S. Miyauchi, "The design of planar circulators for wide-band operation," *IEEE Trans. Microwave Theory Tech.*, vol. MTT-28, no. 3, pp. 210–214, Mar. 1980.

[9] T. Miyoshi, S. Yamaguchi and S. Goto, "Ferrite planar circuits in microwave integrated circuits," *IEEE Trans. Microwave Theory Tech.*, vol. MTT-25, no. 7, pp. 593–600, July 1977.

[10] C. M. Krowne, "Vector variational and weighted residual finite element procedures for highly anisotropic media," *IEEE Trans. Antennas Propagat.*, vol. 42, pp. 642–650, May 1994.

[11] G. G. Gentili and G. Macchiarella, "Efficient analysis of planar circulators by a new boundary-integral technique," *IEEE Trans. Microwave Theory Tech.*, vol. 42, no. 3, pp. 489–493, Mar. 1994.

[12] Y. Ayasli, "Analysis of wide-band stripline circulators by integral equation technique," *IEEE Trans. Microwave Theory Tech.*, vol. MTT-28, no. 3, pp. 200–209, Mar. 1978.

[13] N. Kishi and T. Okoshi, "Proposal for a boundary-integral method without using Green's function," *IEEE Trans. Microwave Theory Tech.*, vol. MTT-35, no. 10, pp. 887–892, Oct. 1987.

[14] T. Okoshi and T. Miyoshi, "The planar circuit—An approach to microwave integrated circuitry," *IEEE Trans. Microwave Theory Tech.*, vol. MTT-20, no. 4, pp. 245–252, Apr. 1972.

[15] H. How, T.-M. Fang, C. Vittoria, and R. Schmidt, "Design of six-port stripline ferrite junction circulators," *IEEE Trans. Microwave Theory Tech.*, vol. 42, pp. 1272–1275, July 1994.

[16] C. M. Krowne, "Theoretical techniques for analyzing nonreciprocal microwave planar devices: Modeling, simulation and relationship to experiment," *Workshop on CAE, Modeling and Measurement Verification*, London, Oct. 1994, pp. 110–115.

[17] ——, "Electromagnetic propagation and field behavior in highly anisotropic media," in *Advances in Imaging and Electron Physics*. New York: Academic, vol. 92, 1995.

[18] H. Bosma, "On stripline Y-circulation at UHF," *IEEE Trans. Microwave Theory Tech.*, vol. MTT-12, pp. 61–74, Jan. 1964.

[19] H. Bosma, "On the principle of stripline circulation," in *Proc. IEE*, pt. B, suppl. 21, Jan. 1962, vol. 109, pp. 137–146.

[20] A. M. Borjak and L. E. Davis, "On planar Y-ring circulators," *IEEE Trans. Microwave Theory Tech.*, vol. 42, no. 2, pp. 177–181, Feb. 1994.

[21] L. E. Davis and V. A. Dmitriyev, "Nonreciprocal devices using ferrite ring resonators," in *IEE Proc.*, June 1992, vol. 139, pt. H, no. 3, pp. 257–263.

[22] J. Helszajn and W. T. Nisbet, "Complex Gyrator circuit of junction circulators using weakly magnetized ring resonators," in *IEE Proc.*, Aug. 1992, vol. 139, pt. H, no. 4, pp. 319–322.

[23] C. M. Krowne, "Fourier transformed matrix method of finding propagation characteristics of complex anisotropic layered media," *IEEE Trans. Microwave Theory Tech.*, vol. MTT-32, pp. 1617–1625, Dec. 1984.

[24] C. M. Krowne, A. A. Mostafa, and K. A. Zaki, "Slot and microstrip guiding structures using magnetoplasmons for nonreciprocal millimeter wave propagation," *IEEE Trans. Microwave Theory Tech.*, vol. 36, pp. 1850–1860, Dec. 1988.

[25] C. M. Krowne, "Waveguiding structures employing the solid state magnetoplasma effect for microwave and millimeter wave propagation," *IEE Proc., Microwaves, Antennas, and Propagat.*, invited review paper for special issue on gyroelectric waveguides and their circuit application, June 1993, vol. 140, pt. H, no. 3, pp. 147–164.

[26] C. M. Krowne and R. E. Neidert, "Inhomogeneous ferrite microstrip circulator: Theory and numerical calculations using a recursive Green's function," in *25th Eur. Microwave Conf. Dig.*, Bologna, Italy, Sept. 4–8, 1995, pp. 414–420.

[27] R. E. Blight and E. Schlömann, "A compact broadband microstrip circulator for phased array antenna modules," in *IEEE MTT-S Int. Symp. Dig.*, 1992, pp. 1389–1392.

[28] R. F. Soohoo, *Theory and Application of Ferrites*. Englewood Cliffs, NJ: Prentice-Hall, ch. 5, 1960.

[29] R. I. Joseph and E. Schlömann, "Demagnetizing field in nonellipsoidal bodies," *J. Appl. Phys.*, vol. 36, no. 5, pp. 1579–1593, May 1965.

[30] C. M. Krowne, "Cylindrical-microstrip antenna," *IEEE Trans. Antennas Propagat.*, vol. AP-31, pp. 194–198, Jan. 1983.

[31] M. G. Mathew and T. J. Weisz, "Microwave transmission devices comprising gyromagnetic material having smoothly varying saturation magnetization," U.S. Patent 4 390 853, June 28, 1983.

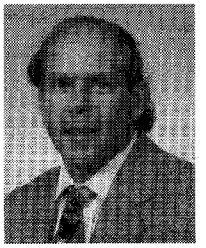

Clifford M. Krowne (S'73–M'74–SM'83) received the B.S., M.S., and Ph.D. degrees at University of California at Berkeley, Davis and Los Angeles.

He has worked in the Microelectronics Division of Lockheed Missiles and Space Company in Sunnyvale, CA, as a Member of the Solid State Technical Staff of the Watkins-Johnson Company in Palo Alto, CA, and as a Faculty Member in the Department of Electrical Engineering at North Carolina State University, Raleigh. Since 1982, he has been with the Microwave Technology Branch, Electronics Science & Technology Division of the Naval Research Laboratory, Washington, DC, studying microwave and millimeter-wave properties of active and passive solid state devices. He also was an Adjunct Professor of Electrical Engineering at the University of Maryland, College Park, MD. He has published 130 conference papers, books, and journal papers, and has several patents on solid state electronics, microwave circuits, electromagnetics, engineering education, and applied physics.

Dr. Krowne has served on the Technical Program Conference Committees of the Antennas and Propagation Society (1983 and 1984) and the Microwave Theory and Techniques Society (1982 to 1996), has chaired sessions in the electromagnetic theory, microstrip antenna, and solid-state devices/circuits, superconductor, and monolithic circuit areas, and organized two MTT-S workshops on 2-D/3-D full wave simulation (1992) and self-consistent particle transport/full wave dynamic field simulation (1993). He was a member of the 1987 MTT Symposium Steering Committee. He is a member of Phi Kappa Phi and Tau Beta Pi and a Fellow of the Washington Academy of Sciences.

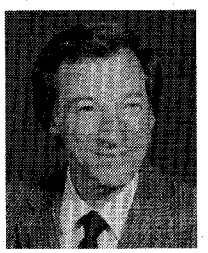

Robert E. Neidert (S'56-M'70) received the B.E. (E.E.) degree in 1959 from Vanderbilt University, Nashville, TN, and has done graduate work at the University of Florida, St. Petersburg.

From 1959 to 1962 he was with the Sperry Microwave Electronics Company, Clearwater, FL, where he was engaged in the development of microwave components for radar systems. From 1962 to 1969 he served as Senior Engineer and Project Leader at the General Electric Company, Communications Products Department, Lynchburg, VA, in the development of microwave components and solid state sources for TV and multiplex telephone radio relay systems. From 1969 to 1972 he was a Principal Engineer at Radiation Systems, Inc., McLean, VA, where he worked in microwave antennas and antenna feed networks. Since 1972 he has been involved in research on microwave and millimeter-wave devices and circuits at the Naval Research Laboratory, Washington, DC. He has authored numerous papers in the fields of communications systems components, microwave integrated circuits, computer-aided microwave circuit design, bipolar and FET amplifier design, FET modeling, millimeter-wave circuits, vacuum microelectronics, and microwave ferrite components.

Mr. Neidert is a member of Tau Beta Pi.